INTERNATIONAL JOURNAL OF PRECISION ENGINEERING AND MANUFACTURING Vol. 16, No. 8, pp. 1833-1843 JULY 2015 / 1833
DOI: 10.1007/s12541-015-0239-2 ISSN 2234-7593 (Print) / ISSN 2005-4602 (Online)

Design and Modeling of an Innovative Wave Energy Converter Using Dielectric Electro-active Polymers Generator

Phan Cong Binh[1], Doan Ngoc Chi Nam[2], and Kyoung Kwan Ahn[3,#]

1 Graduate school of Mechanical and Automotive Engineering, University of Ulsan, 93, Daehak-ro, Nam-gu, Ulsan, 680-749, South Korea
2 Singapore Institute of Manufacturing Technology (SIMTech), Agency for Science Technology and Research (A-STAR), 638075, Singapore
3 School of Mechanical and Automotive Engineering, University of Ulsan, 93, Daehak-ro, Nam-gu, Ulsan, 680-749, South Korea
Corresponding Author / E-mail: kkahn@ulsan.ac.kr, TEL: +82-52-259-2282, FAX: +82-52-259-1680

KEYWORDS: Dielectric Electro Active Polymer (DEAP), WEC, Hydrodynamic model, Structural optimization

This paper proposes a design and modeling of an innovative wave energy converter using Dielectric electro active polymer (DEAP). Firstly, an accurate model of conventional DEAP generator is investigated and validated under a specific range of ocean waves. Then, a structure design of an antagonistic DEAP generator so-called energy capture unit (ECU), which consists of two DEAPs in antagonistic connection mode to increase harvested energy efficiency, is modeled and validated by experimental data. A new design of WECs is then developed with array of ECUs to increase the output energy. In addition, by using the linear potential wave theory, the hydrodynamic forces are calculated under regular wave conditions. Consequently, a complete analytical model of the proposed WECs using multiple ECUs under hydrodynamic behavior is then obtained to investigate the performance of energy conversion. Finally, based on the developed analytical model, the stretch ratio known as an important factor to efficiency and output power is investigated under the influence of the floating buoy's mass. Then, the resonance behavior of the WECs with a typical wave frequency can be tuned by optimizing the floating's mass to increase the degree of utilization of the device. The simulation results indicate that the efficiency of wave energy converter can be up to 25% thanks to resonance behavior.

Manuscript received: September 26, 2014 / Revised: April 22, 2015 / Accepted: May 12, 2015

1. Introduction

Since the oil crisis of 1973, renewable energy has attracted many studies and harvesting energy from vibration sources has been one of the most potential technologies.[1] Among these vibration sources, energy generation from ocean waves has become an extremely promising candidate. Therefore, the wave power technologies have been studied and developed for decade. Falcão AF de O[2] reviewed the development of wave energy utilization since the 1970s. There are relevant topics are presented in this work: the characterization of the wave energy resource, theoretical background, development of specific equipment (air and water turbines, high-pressure hydraulics, and linear electrical generators) and mooring systems, etc. In addition, Iraide Loìpez et al.[3] presented a complete analysis of the wave energy technology. The characterization of the global resource is investigated to show the most suitable places where can exploit equipment. It describes the classification of the different types of WEC. The tendency by companies to develop point absorber type is about 81.78%. Then, the most important development stages of floating point absorber WEC is presented in Ref. 4. Here, the wave energy resource is assessed for a given location. An overview of the mechanism for different wave energy conversion systems is studied. Variations of the power output of the generator and optimum performance of the point absorber are presented correspond to the natural frequency of the device. Various mooring configurations and an overview of scaled modelling are also presented. Moreover, modelling and control strategy techniques of a sea wave energy conversion system were presented by J. Leclerc et al in Ref. 5. An innovative WEC using a floating cylinder coupled with a DC generator is exploited on the shore to reduce maintenance and the electricity transport line costs. Appropriate improvements in the model and the control strategy is implemented to enhance the overall process efficiency. To evaluate the performance of a WEC under regular and irregular wave conditions, Boo Woo Nam et al.[6] carried out a numerical investigation of the hydrodynamic

performance of the floating pendulum WEC which consists of three main components: floater, pendulum and damping plate. The hydrodynamic coefficients and wave exciting forces acting on the buoy are obtained by using the higher-order boundary element method. The effects of the main shape parameters on power absorption and buoy motion were also investigated by numerical model.

Although development of WEC technologies has approached and implemented a significant contribution to energy extraction from ocean waves, there still exist some challenges to be addressed. One of the most significant drawbacks in current WEC system is the use of a complex mechanical structure or a low efficiency hydraulic system to transmit and convert the fluctuating large load with low frequencies of wave motion into the significant smaller load at higher frequencies of electromagnetic generators.[7] Therefore, studies on a direct-drive technology for WECs with simpler structure and low operation frequency (0.05-0.5 Hz) are necessary.

Thanks to the development of smart materials and structure, there have been three main functional materials which can be applied to energy harvesting field: piezoelectric, dielectric elastomer, and the composite material combining polymer and piezoelectric ceramic. Piezoelectric materials usually work under high frequencies and low deformation.[8,9] On a different trend, the dielectric elastomer (DE), which has been known as polymer or compliant capacitor, is a new technology that can be applied in WECs thank to its low cost, lightweight, simple actuating structure and good performance in low frequencies with large deformation. Finally, a composite material combining polymer and piezoelectric ceramic properties was designed to fulfill the operating requirements for integration in automobile tires.[10]

A typical DE film includes a soft dielectric elastomer which is sandwiched between two compliant electrode layers.[11] There are several works involving on the basic working principle.[12-14] Fundamentals of dielectric elastomer in generator, actuator, and sensor mode are described in these works. In the actuator mode, electrical energy is converted into mechanical work by bringing opposite charged layers closer together. Inversely, in the generator mode, mechanical work is converted into electrical energy using the polymer's capacitive behavior.

The generator mode has gained more attention recently. A simple dynamic model and comparisons between several energy harvesting cycles were reported in Ref. 15. Soft capacitors for wave energy harvesting including realistic theoretical and numerical model were investigated to optimize electric circuit, dielectric and mechanical material parameters.[16] Development a solution for artificially increasing the coupling factor of electrostrictive materials based on the optimizing the frequency of the electric field and the amplitude strain of the mechanical excitation were studied to increase in the generated current.[17] Graf C et al developed a polyurethanes which have certain advantages over silicones and acrylates.[18] The energy gain and other important material parameters had been optimized to fit the requirement for energy converter. Some works investigated the performance of DE generator based on energy conversion cycle. For example, circular energy conversion unit was implemented to carry out experiment in Ref. 19. The test results indicated that the bias voltage and stretch displacement have effect onto the efficiency and the output power significantly. Several tests using a simple scale model EPAM in wave energy harvesting system were carried out in a water tank, and the results showed that the output energy depends largely onto wave period.[20]

In addition, some authors have studied different modeling techniques. Graf C et al presented a simulation model for DE generators which combines the electrostatic properties and the nonlinear elastic behavior (the Neo-Hookean stress-strain model) of the polymer material.[21] A biaxial plane generator using a dielectric polymer was developed in Ref. 22. Here, a reliable method for generator modelling was proposed and validated by experiments. Then, the structure was optimized with material properties constraints. In another attempt, Antoniadis A et al presented dielectric elastomer energy generating synergetic structures (DIESYS) which connect two elementary characteristic DIESYS design concepts for in-plane and out-plane oscillations.[23] The Neo-Hookean model was also employed to describe non-linear broad-band system response in this work.

Most of previous studies of DE materials in the generator mode have shown favorable results under laboratory condition. The main purposes of these works involve in optimization energy harvesting cycles to increase conversion efficiency and output power. DE material properties were studied to fit the requirement for energy converter and to decrease the losses. Test results indicated the stretch ratio as a significant factor affect to the harvested energy; meanwhile these values were prescribed in advance precisely. However, for wave energy converter using DE, stretch ratio must be determined by solving the equation of motion which combines the hydrodynamic force coupled with the DEAP forces. Consequently, stretch ratio would be optimized to maximize output power and to prevent mechanical breakdown.

This paper presents an innovative design of WECs using an array DEAPs with floating buoy's mass configuration for higher energy efficiency. Firstly, modeling of DEAP material in generator mode is presented. Here, the Mooney-Rivlin strain model along with two sets of DEAP parameters is employed to describe electromechanical behavior of DEAP generator. This model is then validated by experiment under low operating frequencies of the wave excitation force. Secondly, in order to scavenge the pre-strain energy and the returned energy, a design concept of an energy capture unit (ECU) is proposed, and a simulation model is developed to investigate the induced force in term of stretch ratio. Then, the model is validated by a reasonable agreement between simulation and measurement results. Next, a complete analytical model of the energy capture unit (ECU) coupling with hydrodynamic behavior is calculated under the regular wave conditions. The hydrodynamic forces including the excitation force, radiation impedance, viscous and hydrostatic force, are presented by using the linear potential wave theory. Then, structural optimization for ECU is calculated to increase the degree of utilization of the device and to optimize stretch ratio. By adjusting the mass of floating buoy, the natural frequency of the device is turned close to the excitation force frequency (resonance behavior). Mass adjusting mechanism is introduced in an innovative design of the floating buoy. Finally, a numerical simulation is built in MATLAB/ Simulink to investigate performances of ECU under hydrodynamic behavior. By setting some parameters, simulation results indicates that stretch ratio can be adjusted to optimize the utilization of wave energy. Consequently, the efficiency of the WECs can be increased significantly thanks to resonance behavior.

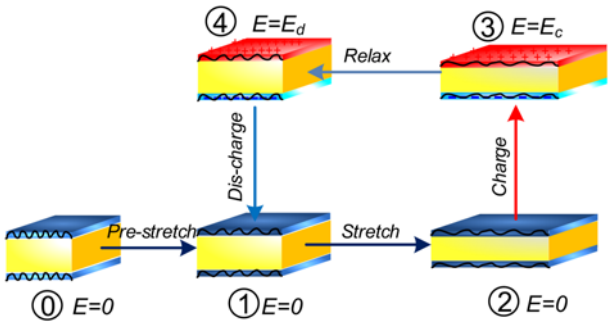

Fig. 1 Basic working principle of DEAP energy cycle

2. Energy Harvesting Principle

There are several energy cycles which can be used to produce electrical energy from DEAP material.[14] In this work, for simplicity, we present one energy cycle based on a constant charge Q. The basic operating principle of DEAP generator in an energy harvesting cycle is generally described in Fig. 1. Here, DEAP material is usually pre-stretched to decrease the charging voltage and increase the efficiency (phase 0-1). Because DEAP acts like variable capacitor (compliant capacitor), stretching DEAP causes reduction in thickness and increasing the surface area (phase 1-2). Its capacitance is varied as a well-known equation:

$$C = \varepsilon_r \varepsilon_0 \frac{S}{t} = \varepsilon_r \varepsilon_0 \frac{B}{t^2} \tag{1}$$

where ε_0 is the permittivity of free space (8.85×10^{-12} F/m), ε_r is the relative dielectric constant of DEAP, S is the active electrode surface, t and B are the thickness and volume of DEAP material, respectively.

At the point 2, a pre - charge $Q = CV_c$ is placed upon the two electrode layers where positive charges are on one side and negative ones are one the other side. Due to the Coulomb's law, an electric field is induced between two electrode layers. Consequently, stress, due to electrostatic force, is given in Ref. 23, and can be expressed in Eq. (2). It is assumed that only electrostatic phenomenon is represented.

$$\sigma_{me} = \varepsilon_0 \varepsilon_r E^2 \tag{2}$$

where E is the magnitude of the electric field describing the electrostatic phenomenon.

At this moment, the input energy into DEAP can be given in the following equation:

$$e_1 = 0.5 C_c V_c^2 \tag{3}$$

where C_c and V_c are the capacitance and the voltage between two electrode layers, respectively. On path 3-4, the DEAP material is allowed to contract to point 4 based on the equilibrium between the elastic recovering force and the electrostatic force. Then, the stored energy in DEAP at this point is expressed in Eq. (4):

$$e_2 = 0.5 C_d V_d^2 \tag{4}$$

where C_d and V_d are is the capacitance and the voltage on two electrode layers, respectively.

Finally, the output energy of DEAP generator per cycle defined as the difference between Eqs. (4) and (3) and is obtained in Eq. (5)

$$e_{cyc} = e_2 - e_1 = 0.5 C_c V_c^2 (C_c/C_d - 1) \tag{5}$$

The second equality in above equation can be written because charge $Q = VC_c$ is essentially constant.

3. Modeling of DEAP Material in Generator Mode

In order to describe DEAP mechanical behavior, a complete model including mechanical coupling electrical system is presented by Ref. 26. The equation of motion in term of stretch ratio is expressed in the set of Eq. (6).

$$\begin{gathered} m_{eq} l_0 \frac{d^2 \lambda_x}{dt^2} = F_e(t) - F_{el}(\lambda_x) + F_{me}(\lambda_x) \\ \lambda_x = \frac{l_x}{l_0} = 1 + \alpha \end{gathered} \tag{6}$$

where m_{eq} is an equivalent mass includes attached mass of a support system and half of DEAP material mass; l_x and l_0 are the current and the initial length, respectively; λ_x and α are stretch ratio and the strain of DEAP generator, respectively; $F_e(t)$, F_{el} and F_{me} is an excitation force, an elastic recovering force and Maxwell force, respectively.

For calculation the elastic recovering force, the Mooney-Rivlin model is employed to describe stretch and force relationship. Stress in term of stretch ratio was given in Refs. 24 and 26, and expressed in Eq. (7). Then, the elastic recovering force is obtained by multiplying results of Eq. (7) and current section area in Eq. (8).

$$\sigma_{el} = 2\left(C_1 + \frac{C_2}{\lambda}\right)\left(\lambda^2 - \frac{1}{\lambda}\right) \tag{7}$$

$$F_{el} = w_0 t_0 \left[2\left(C_1 + \frac{C_2}{\lambda}\right)\left(\lambda - \frac{1}{\lambda^2}\right)\right] \tag{8}$$

where C_1 and C_2 are DEAP material parameters; w_0 and t_0 are initial width and thickness respectively.

The Maxwell force can be obtained by multiplying the results of Eq. (4) and current section area $S_x = wl$, and expressed in Eq. (9):

$$F_{me} = \varepsilon_0 \varepsilon_r \frac{w_0 V_c^2 \lambda}{t_0} \tag{9}$$

Substituting Eqs. (8) and (9) into Eq. (6), the coupled equation of motion can be obtained as follow:

$$M_{eq} l_0 \ddot{\lambda} + w_0 t_0 \left[2\left(C_1 + \frac{C_2}{\lambda}\right)\left(\lambda - \frac{1}{\lambda^2}\right)\right] - \varepsilon_0 \varepsilon_r \frac{w_0 V_c^2 \lambda}{t_0} = F_e(t) \tag{10}$$

Material parameters C_1 and C_2 can be determined by curve fitting experiment results with Eq. (10). Training data consisting of stretch ratios and response forces are obtained by measuring directly. Then, these data are used to optimize material parameters C_1 and C_2 using a standard tool 'lsqcurvefit' in Matlab/Simulink. As results, two different sets of DEAP parameters are obtained in stretch and relaxation phase separately to describe viscous behavior under the narrow range of operating frequencies. In order to validate this model, a simple test rig was set up. Here, specification of DEAP material and experimental

Table 1 Specification of DEAPs generator

Parameters	Value
t_0	80×10^{-6} m
w_0	2 m
l_0	0.18 m
ε_0	8.85×10^{-12} F/m
ε_r	3.1
E_{max}	40×10^{6} V/m
DEAPs mass	0.0297 kg

Table 2 Experimental parameters for identification procedure

Parameters	Value
Operating environment	Dry environment
Operating frequency	0.5 Hz
Sampling time	0.01s
Maximum stretch ratio	122.5%
m_{eq}	0.7 kg
Gravitational acceleration	9.81 m/s^2

Table 3 DEAP parameters from the tensile test and relaxation

Parameters	Stretch stroke	Relax stroke
C_1 (Pa)	4.52e5	2.53e5
C_2 (Pa)	-3.52e5	-1.18e5

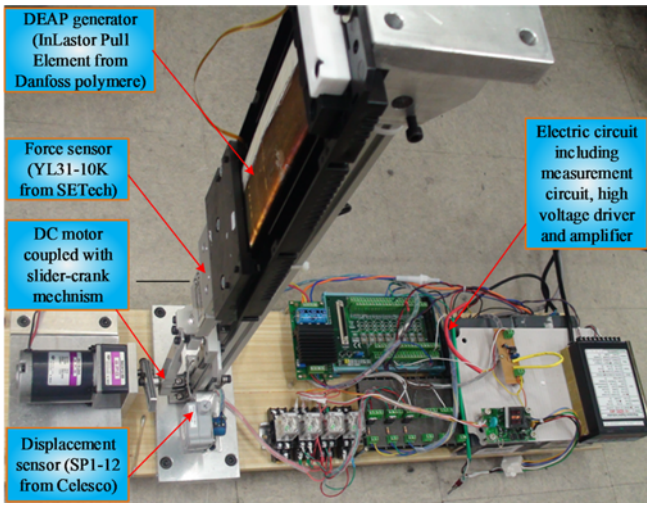

Fig. 2 Experimental setup for DEAP model

parameters are shown in Table 1 and Table 2, respectively. Then, set of material parameters C_1 and C_2 are determined and shown in Table 3. For general case, Michael W et al determined time dependent material parameters by using Prony series in Ref. 25. However, for a specific case such as small stretch ratio and narrow range of operating frequencies, the proposed method is simpler than that of;[25] meanwhile the accuracy of model is acceptable.

Substituting material parameters into Eq. (10), a response force is obtained to compare with that of experiment. A test rig for experiment is illustrated in Fig. 2, and experimental results are plotted in Fig. 3. Although a narrow range (0.1-1 Hz) has been investigated for validation, for simplicity, only 0.5 Hz operating frequency results is shown in this figure. The test results indicated that the proposed model can be validated, thank to small relative error (<5%).

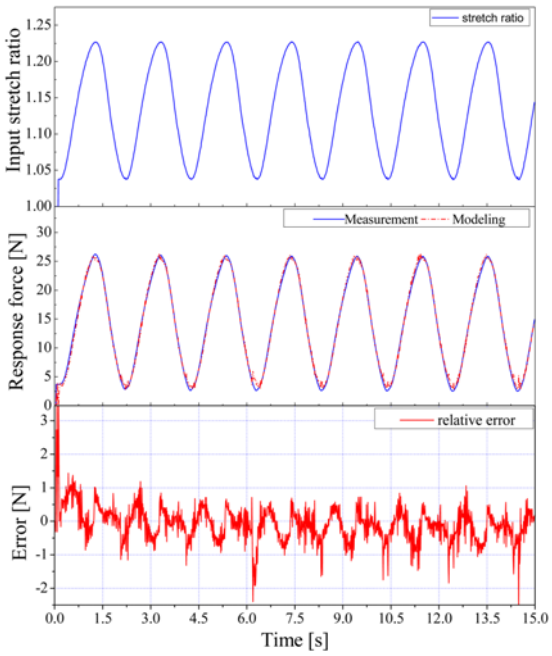

Fig. 3 Response force comparisons between simulation and measurement results under 0.5 Hz and 1300 V charged voltage.

4. An Innovative Design of a WEC System

4.1 Design concept & working principle

The general concept of the proposed WEC is depicted in Fig. 4 which consists of five main components: a platform, energy capture unit (ECU), a floating buoy, a balloon chamber and a sea water pump. The platform is held stationary relative to free water surface on the sea and fixed to ECU at one end. Multi ECUs are assembled in circular array on the platform axis symmetrically. The other ends of these ECU are also fixed on the other floor of the platform. Each ECU consists of two DEAP generators, which are in antagonistic connection and shown in Fig. 5. The truncated vertical cylinder buoy with a hemisphere at the lower end is employed to decrease viscous. The buoy is linked to the platform by a guideline shaft. Other smaller shafts are fixed their one end on the floating buoy, and the other ends are fixed to ECU at midpoint between two DEAP generators. The balloon chamber with pre-charged pressure is mounted inside the floating buoy.

The main purpose of this design is to convert the wave energy into electrical energy in high efficiency. Moreover, the output energy can be optimized by calculating the quantity of ECUs, and the maintenance can be done by replacing ECUs easily. For each ECU, the pre-stretch process to equilibrium position is carried in advance. Therefore, the pre-stretch energy is not taken into account, and the mechanical energy can be converted to useful electrical energy without loss for pre-stretched energy.

Reacting to the incident waves, the floating buoy is forced to oscillate up and down. Consequently, DEAP generators are also stretched and relaxed. Due to antagonistic connection, one DEAP generator is stretched; meanwhile the other DEAP is allowed to retract. On the other hand, the elastic force of one DEAP generator in relaxing phase is used to stretch the opposite one. Thus, the required forces

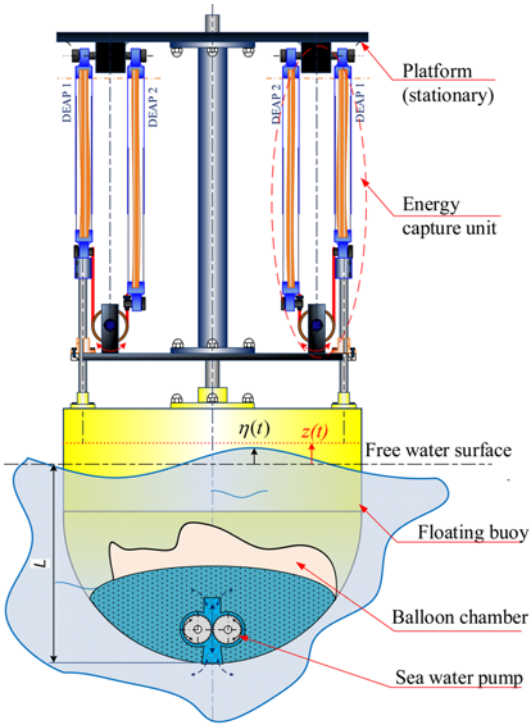

Fig. 4 The proposed structure of WEC assembled multiple ECU

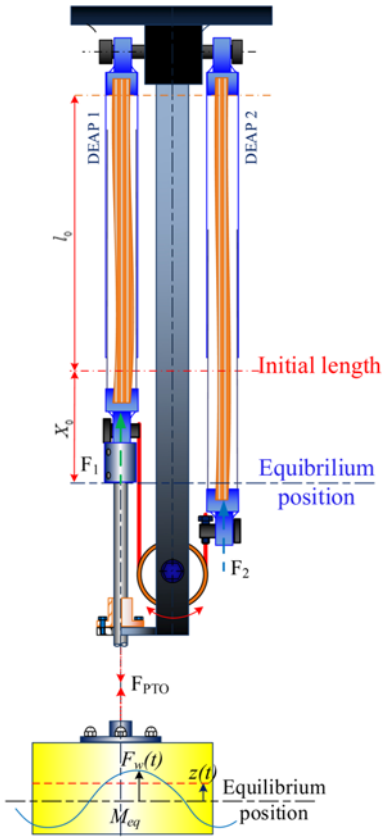

Fig. 5 Schematic of the ECU

using to operate ECU are reduced under the same stretch ratio. Then, the energy conversion efficiencies can be increased significantly.[27]

For maximum absorbed energy, the inertia of the floating buoy structure must be tuned to values that bring the natural frequencies of device close to wave spectrum frequencies (resonances behavior). A bidirectional seawater pump is employed to change floating buoy's mass by pumping water into the chamber or outside environment. The pre-charged pressure inside the balloon chamber keeps water stable to reduce the influence of hydrodynamic behavior inside chamber. In literature, the floating buoy can be split into two parts,[28] one is closed to the water surface to have good radiation capabilities, and the other one is submerged deep enough to not affect the radiated wave from the surface buoy.

4.2 Mathematical model

In order to investigate the performance of the proposed WEC under the hydro-mechanical dynamic behavior, a schematic is shown in Fig. 5. Here, the forces acting on the floating buoy consist of the reactive force, due to power take-off system (PTO), and the hydrodynamic forces, due to the incident wave.[29] The behavior of the buoy is analyzed as a single body system with one degree of freedom along the vertical z-axis.[30] According to the Newton second's law, the equation of floating motion is expressed in Eq. (11):

$$M_{eq}\ddot{z} = F_w + F_{PTO} \tag{11}$$

where $F_w(t)$ is the hydrodynamic force that can be calculated by the following equation:

$$F_w(t) = F_e(t) + F_r(t) + F_v(t) + F_s(t) \tag{12}$$

where $F_e(t)$ is the excitation force, which is usually decomposed in two components: Froude-Krylove force and the diffraction force.[31] Here, the Froude-Krylove force is caused by the undisturbed wave field and can be represented for the excitation force. The diffraction force can be negligible due to the small floating buoy compared with wavelength and small phase difference. The excitation force $F_e(t)$ is simplified by:

$$F_e = \kappa\rho g\pi a^2\eta \tag{13}$$

where κ is the hydrodynamic parameter for the heave mode of a floating truncated vertical cylinder of radius a, which is computed by using a method of Eidsmoen, or can be obtained by using non-dimensional graphs;[30] ρ is the density of sea water; η is wave elevation.

$F_r(t)$ is the radiation damping force which is induced by buoy oscillations, and expressed in the set of Eq. (14)

$$\begin{aligned} F_r &= -m_a\ddot{z}(t) - R_r\dot{z}(t) \\ m_a &= \mu_r M_{eq} \\ R_r &= \varepsilon_r M_{eq} \end{aligned} \tag{14}$$

where $z(t)$ is the displacement of the buoy; m_a is the added mass and R_r is the radiation damping coefficient; μ_r and ε_r are the hydrodynamic parameters which are depended the body geometry and working condition on the ocean, and can be determined by using the graphs (versus the coefcient ka).

$F_v(t)$ is the viscous damping force, due to relative turbulent flow, and can be calculated by:

$$F_v(t) = -\frac{1}{2}\rho C_{dr}A_d(\dot{z}-\dot{\eta})|\dot{z}-\dot{\eta}| \tag{15}$$

where C_{dr} is drag coefcient and A_d is the water plane area of the buoy at rest.

$F_s(t)$ is the hydrostatic restoring force, due to excursion of the buoy from its equilibrium position, which can be calculated by using the Archimedes principle, and is simply given in the set of Eq. (16):

$$\begin{aligned} F_s &= -S_b z \\ S_b &= \rho g \pi a^2 \end{aligned} \tag{16}$$

where S_b is the so-called the hydrostatic stiffness.

Substituting Eqs. (13)~(16) into Eq. (12), the hydrodynamic force is obtained in Eq. (17)

$$\begin{aligned} F_w(t) = \kappa \rho g \pi a^2 \eta - \mu_r M_{eq} \ddot{z}(t) - \varepsilon_r M_{eq} \dot{z}(t) \\ --\frac{1}{2}\rho C_{dr} A_d (\dot{z}-\dot{\eta})|\dot{z}-\dot{\eta}| - \rho g \pi a^2 z \end{aligned} \tag{17}$$

F_{PTO} is the PTO force which couples the electromechanical forces of the 1st and 2nd DEAP generator. As shown in Fig. 4, F_{PTO} is calculated by:

$$F_{PTO} = -F_1(\lambda_1) + F_2(\lambda_2) \tag{18}$$

where $F_1(\lambda_1)$ and $F_2(\lambda_2)$ are the electromechanical forces of the 1st and 2nd DEAP generator, respectively. Once $\lambda = \lambda_1$ is defined as stretch ratio of the 1st DEAP generator, λ_2 can be obtained in term of λ in the set of Eq. (19)

$$\begin{aligned} \lambda_2 &= 2S_e - \lambda \\ S_e &= \frac{l_0 + X_0}{l_0} \end{aligned} \tag{19}$$

where S_e and X_0 are stretch ratio and displacement of DEAP generator at the equilibrium position, respectively; l_0 is the initial length of DEAP generator.

Finally, $F_1(\lambda_1)$ and $F_2(\lambda_2)$ can be re-written in term of λ in the set of Eq. (20)

$$\begin{aligned} F_1(\lambda) &= w_0 t_0 \left[2\left(C_1 - \frac{C_2}{\lambda}\right)\left(\lambda - \frac{1}{\lambda^2}\right)\right] - \varepsilon_r \varepsilon_0 \frac{w_0 V_c^2 \lambda}{t_0} \\ F_2(\lambda) &= 2 w_0 t_0 \left(C_1 - \frac{C_2}{2S_e - \lambda}\right)\left(2S_e - \lambda - \frac{1}{(2S_e-\lambda)^2}\right) \\ &\quad - \varepsilon_r \varepsilon_0 w_0 \frac{V_c^2 (2S_e - \lambda)}{t_0} \end{aligned} \tag{20}$$

Substituting Eq. (20) into Eq. (18), the PTO force F_{PTO} is re-written by follow:

$$\begin{aligned} F_{PTO} = 2 w_0 t_0 \left[\left(C_1 + \frac{C_2}{2S_e - \lambda}\right)\left(2S_e - \lambda - \frac{1}{(2S_e-\lambda)^2}\right) \right. \\ \left. - \left(C_1 + \frac{C_2}{\lambda}\right)\left(\lambda - \frac{1}{\lambda^2}\right)\right] + 2\varepsilon_0 \varepsilon_r \frac{w_0 V_c^2}{t_0}(\lambda - S_e) \end{aligned} \tag{21}$$

In order to validate the simulation model Eq. (21), a test bench for experiment is implemented and shown in Fig. 6. Two DEAP generators are antagonistic connected at one end, while the other ends are fixed to above platform. A DC motor coupled with slider-crank mechanism is employed to actuate these DEAP generators. A load sensor and a displacement sensor are used to measure the response forces and displacement in the real time. An electric circuit is also installed to place the charging voltage on two electrode surfaces of DEAP material. Finally, response force comparisons between measurement and model

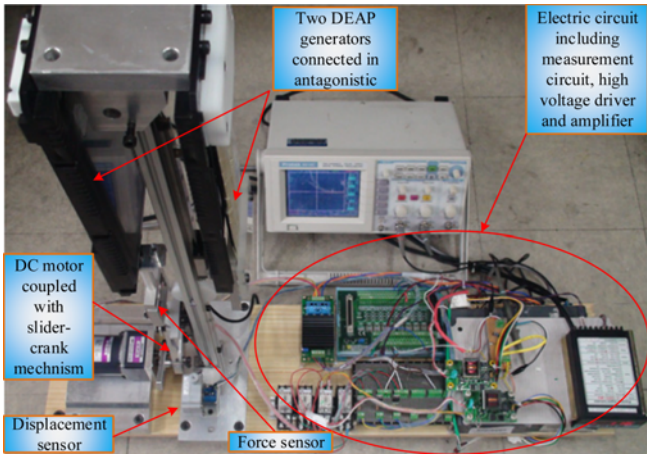

Fig. 6 Experiment setup for two DEAP generators with antagonistic connection

Eq. (21) are shown in Fig. 7. It shows that good agreement between model Eq. (21) and experiment data is found due to small relative error (<5%).

Then, the complete motion equation of floating buoy is obtained by substituting Eqs. (21), (17) into Eq. (12), and it is expressed in the set of Eq. (22):

$$\begin{aligned} &(1+\mu_r) M_{eq} \ddot{z} - \varepsilon_r M_{eq} \dot{z}(t) - \frac{1}{2}\rho C_{dr} A_d (\dot{z}-\dot{\eta})|\dot{z}-\dot{\eta}| - \rho g \pi a^2 z \\ &= \kappa \rho g \pi a^2 \eta - 2\varepsilon_0 \varepsilon_r \frac{w_0 V_c^2}{t_0}(\lambda - S_e) \\ &-2 w_0 t_0 \left[\left(C_1 + \frac{C_2}{2S_e - \lambda}\right)\left(2S_e - \lambda - \frac{1}{(2S_e-\lambda)^2}\right) - \left(C_1 + \frac{C_2}{\lambda}\right)\left(\lambda - \frac{1}{\lambda^2}\right)\right] \\ &\lambda = S_e - z/l_o \end{aligned} \tag{22}$$

5. Structural Optimization for the Floating Buoy

As introduced, in order to maximize the absorbed energy, the natural frequency of PTO devices ω_n must be close to wave frequency ω (resonance condition).[31] For the given WEC, the natural frequency is calculated in the following equation:

$$\omega_n = \sqrt{\frac{S_b + K_{eq}}{(1+\mu_r) M_{eq}}} \equiv \omega \tag{23}$$

where K_{eq} is equivalent stiffness of PTO device and defined as:

$$K_{eq} = \frac{|F_{PTO}|}{z} \tag{24}$$

At equilibrium position on free water surface, the floating buoy is suspended with draft L. Then, M_{eq} can be determined by the following equation:

$$M_{eq} = \frac{2}{3}\rho \pi a^3 + \rho \pi a^2 (L - a) \tag{25}$$

Optimization values of L can be derived by substituting Eqs. (24)

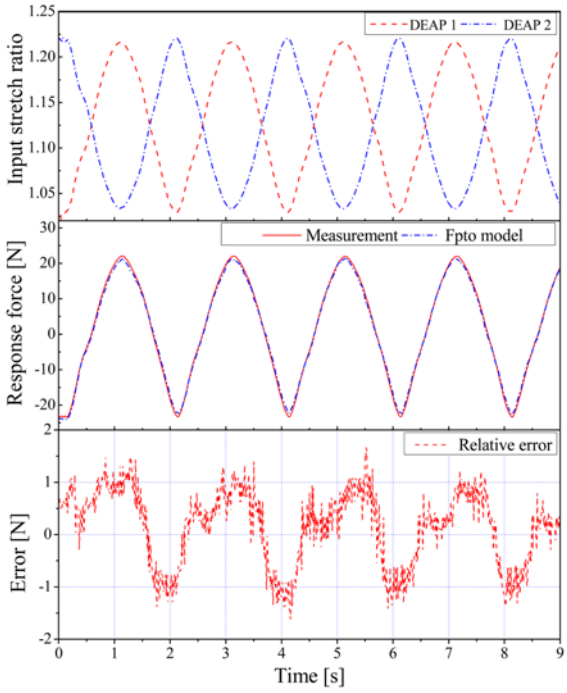

Fig. 7 Response force comparisons between simulation F_{PTO} and measurement results

and (25) into Eq. (23), and its result is obtained by:

$$L = \frac{S_b + K_{eq}}{(1+\mu_r)S_b\omega^2/g} + \frac{a}{3} \tag{26}$$

Once radius of floating buoy is pre-designed, the submerged length L is determined by Eq. (26).

6. Energy Conversion Efficiencies

For the given regular wave, the average wave power is given by Ref. 30, and re-written in Eq. (27):

$$e = e_k + e_p = \frac{1}{8}\rho g^2 H^2 \ , \ (\mathrm{J/m^2}) \tag{27}$$

where e is the mean wave energy density per unit horizontal area which is the sum of kinetic e_k and potential energy e_p; c_g is the group velocity which can be obtained by constant water depth in the set of equations:

$$\begin{aligned} c_g &= \frac{D(kh)}{2\tanh(kh)} c_p = \frac{g}{2\omega} D(kh) \\ D(kh) &= \left[1 + \frac{2kh}{\sinh(2kh)}\right]\tanh(kh) \end{aligned} \tag{28}$$

where $D(kh)$ is the depth function; h is the water depth and k is the angular repetency (wave number) which is defined by: $k = 2\pi/\lambda$

The time dependency of average potential wave energy is obtained by integrating Eq. (27) over time domain:

$$e_w = \int_0^t P_w \ , \ (\mathrm{J}) \tag{29}$$

In analogy with Eq. (29), the time dependency of total theoretical harvested energy is obtained by integrating Eq. (5) over time domain:

$$e_{har} = \int_0^t e_{cyc} \ , \ (\mathrm{J}) \tag{30}$$

Finally, the total efficiencies of the proposed WEC defined by ratio of Eqs. (30) and (29) is obtained in Eq. (31)

$$\zeta_{har} = \frac{e_{har}}{e_w} \tag{31}$$

Table 4 Setting parameters for simulation

Parameters	Value
a	0.25 m
h	9 m
V_c	1300 V
Case 1: η_1	0.005sin(2.244t) m
Case 2: η_2	0.004sin(πt) m

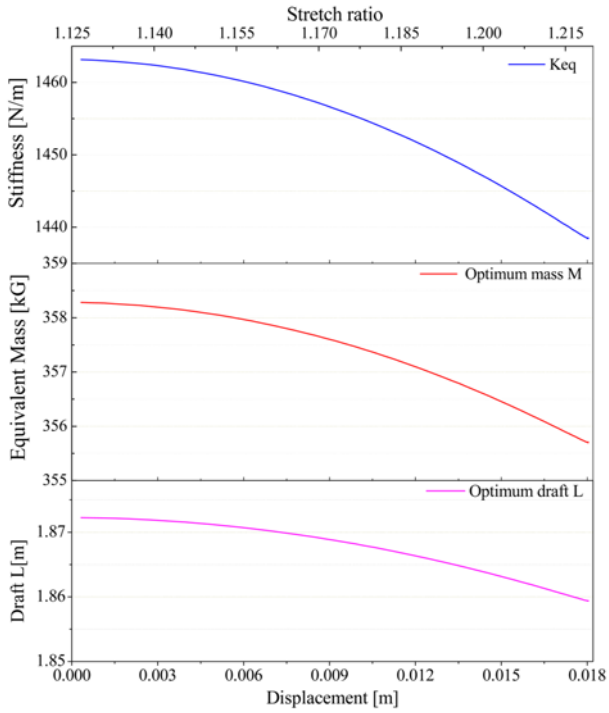

Fig. 8 Simulation results of the equivalent stiffness, the optimum buoy mass and draft under case 1 of wave

7. Simulation Results and Discussions

In order to investigate the performance of the proposed WEC, a numerical model is built in MATLAB/Simulink based on Eq. (22). Simulation is performed under two regular waves with different wave amplitudes and frequencies which are given in Table 4. Then, Eq. (22) is solved by an ODE4 (Runge-Kutta) method with fixed step 0.01 s to determine the buoy elevation. Then, stretch ratio in term of buoy elevation z is obtained. Next, the equivalent stiffness, the optimum mass and the optimum draft are obtained by using Eqs. (24), (25) and

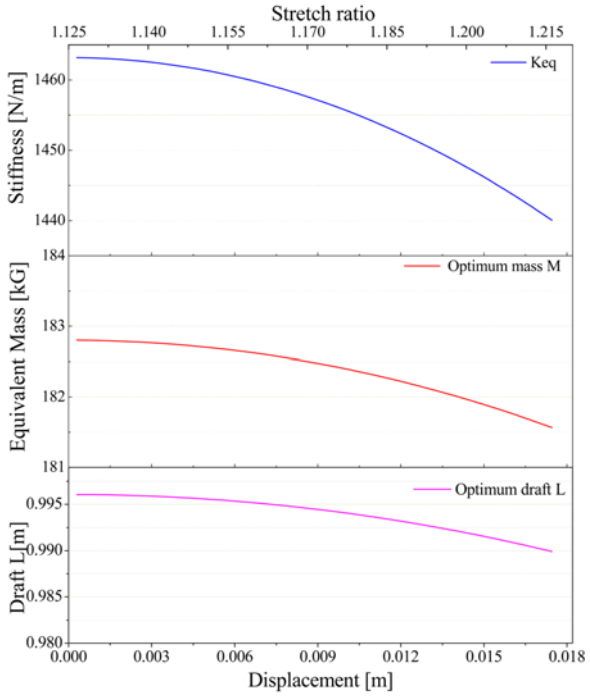

Fig. 9 Simulation results of the equivalent stiffness, the optimum buoy mass and draft under case 2 of wave

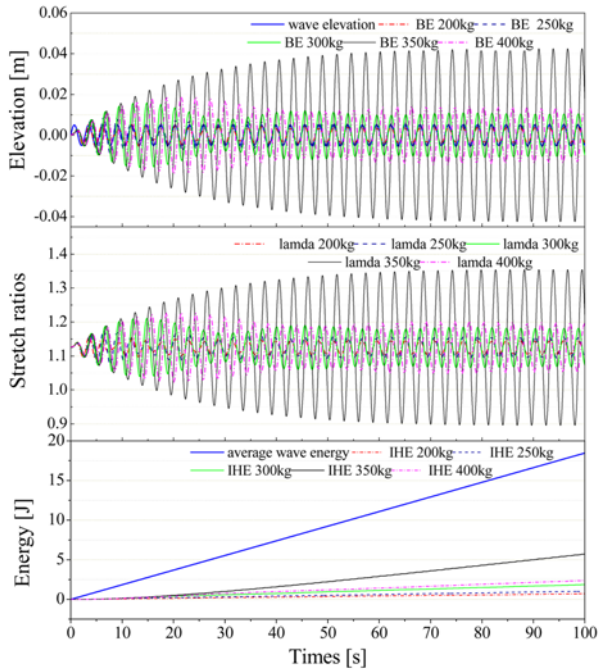

Fig. 10 Buoy elevations, stretch ratios and total theoretical harvested energy for various equivalent masses: 200 kg, 250 kg, 300 kg, 350 kg and 400 kg; under case 1 of wave

(26), respectively. Finally, simulation results under case 1 and case 2 are plotted in Figs. 8 and 9, respectively.

As shown in Fig. 8, a quarter of ideal stretch ratio is investigated to determine optimum values of the stiffness, mass and draft for a given wave frequency. It is clarified that the optimum values are not constant due to nonlinear behavior of DEAP material.

In Fig. 9, the equivalent stiffness is the same, but the equivalent mass and draft is smaller compared to that of Fig. 8. At the same stretch ratios, the reactive forces obtained by Eq. (21) are the same, whereas the equivalent mass and draft are strongly dependent on excitation frequencies. Once wave frequency is increased, the optimum mass and draft must be decreased to tune the device into resonance zone with higher wave frequency.

When optimum floating buoy mass is determined, various mass values bounded this value are selected to simulate the performance of device. Then, simulation results are shown in Figs. 10 and 11.

In Fig. 10, floating buoy elevations under different masses are plotted in the top floor. As shown, at M_{eq} = 350 kg, the buoy elevation has the highest amplitude thanks to resonance behavior. Therefore, stretch ratio and the harvested energy are also the highest values. In theoretical vibration, these results are reasonable agreement. However, due to limitation of stretch ratio for mechanical breakdown DEAP, the buoy mass must be selected to satisfy maximum stretch ratio in the steady state. Some values around of the resonance region in both sides decreases the buoy elevation amplitude. Thus, stretch ratio and the ideal harvested energy are also decreased.

In analogy with Fig. 10, the simulation results under the wave of case 2 are shown in Fig. 11. Here, simulations are carried out by changing mass from 100 kg to 250 kg with step 50 kg. One more simulation is also performed at M_{eq} = 182 kg which can bring the

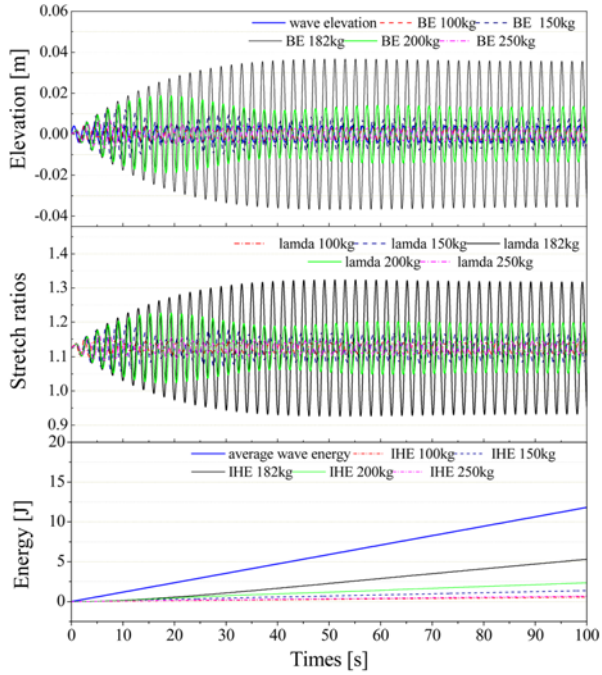

Fig. 11 Buoy elevations, stretch ratios and total theoretical harvested energy for various equivalent masses: 100 kg, 150 kg, 182 kg, 200 kg and 250 kg under case 2 of wave

natural frequency to the resonance region. Apparently, the optimum mass in case 2 is smaller than that of case 1 in Fig. 10. Therefore, the optimum mass is decreasing when the wave frequency is increasing according to Eq. (23).

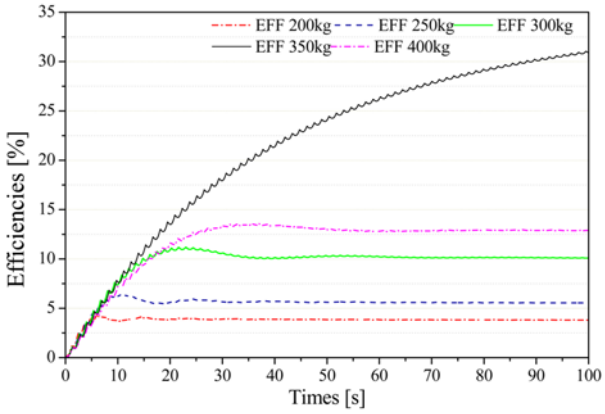

Fig. 12 Change in the total efficiencies under different equivalent masses: 200 kg, 250 kg, 300 kg, 350 kg and 400 kg under wave in case 1

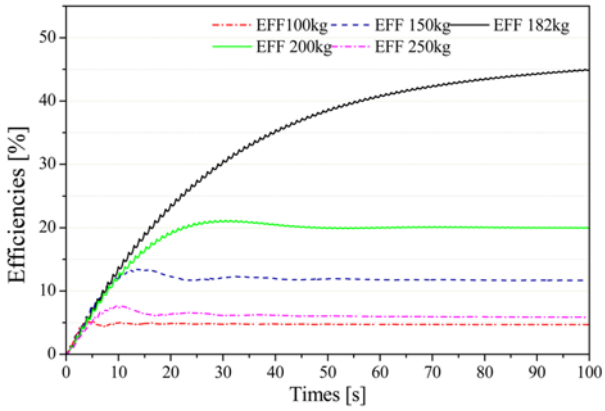

Fig. 13 Change in the total efficiencies under different equivalent masses: 100 kg, 150 kg, 182 kg, 200 kg and 250 kg under wave in case 2

According to Eq. (31), total efficiency is investigated under different masses and plotted in Figs. 12 and 13 for case 1 and case 2 of wave, respectively. In case 1 of wave, total efficiency can be found more than 32% thanks to resonance behavior. And, more than 45% efficiency in wave energy conversion can be reached in case 2 of wave in theory. In realistic, stretch ratio must be satisfied the mechanical breakdown limitation of DEAP material. Therefore, for the given wave, the mass must be tuned to reach the maximum stretch ratio of the given material. For example, in this study, maximum stretch ratio of DEAP material is about 1.22. The ideal performance at steady state for two case of waves are shown in Figs. 14 and 15.

In Figs. 14 and 15, although there is little overshoot at the transient period, maximum stretch ratios are stable in steady-state (from 80 s). Then, the ideal harvested energy (without frictional losses) are shown in the middle of these figures. The same harvested energy (3 J) can be found in two cases of wave due to the same ideal stretch ratio. Since the total wave energy in case 1 is larger than case 2, the total efficiency in case 1 (about 16.7%) is smaller that of case 2 (about 25%). Total

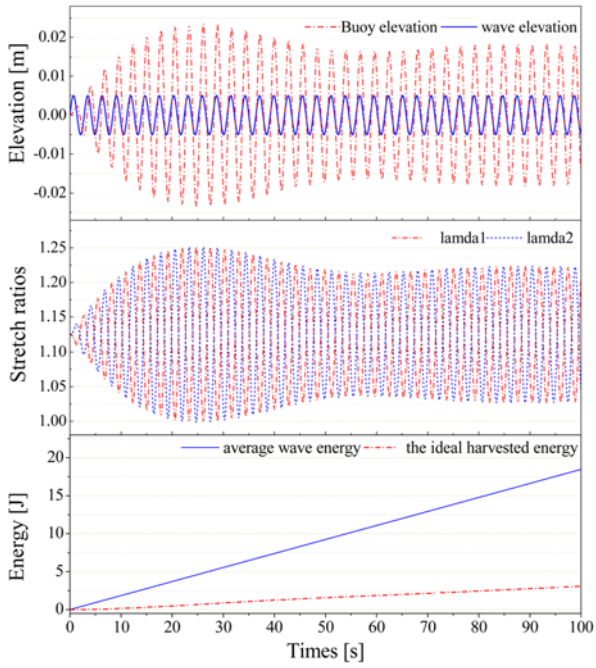

Fig. 14 The ideal performance of the proposed WEC under wave elevation $\eta = 0.005\sin 2.244t(m)$ at $M_{eq} = 335$ kg

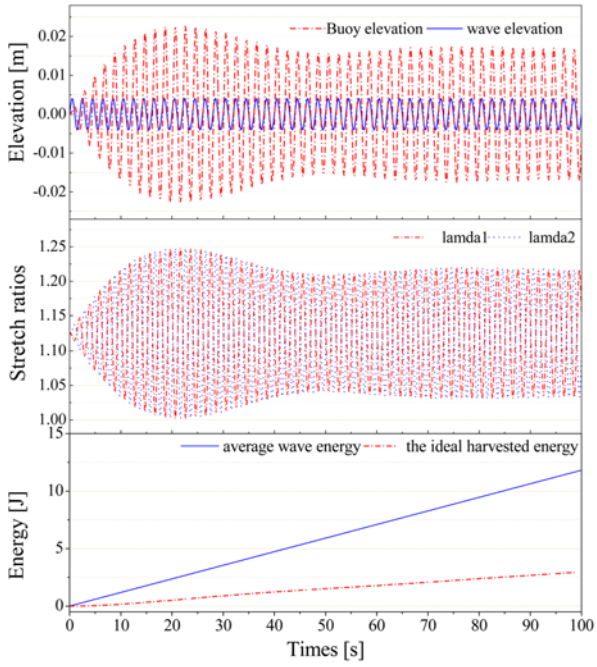

Fig. 15 The ideal performance of the proposed under wave elevation $\eta = 0.004\sin \pi t(m)$ at $M_{eq} = 168$ kg

efficiency difference involves in the reactive force F_{PTO} which can also be controlled to adapt a given incident wave by changing number of ECU. In this study, only one set of ECU is employed to calculate the harvested energy, hence the ideal harvested energy efficiencies are different in two cases of simulation.

8. Conclusion and Future Works

This paper proposed an innovative design concept of WEC using DEAP material. A numerical model of the proposed WEC under hydrodynamic behavior was built to investigate the performance under two regular waves (different wave amplitudes and frequencies) and equivalent masses.

Firstly, simulation model for DEAP behavior is presented and validated by a reasonable agreement with experimental results.

Then, the coupled model including the hydrodynamic forces and the resistive force from the PTO system is built in Matlab/Simulink to investigate the performance of the device.

Next, structural optimization is presented by using the wave linear theory. Simulation results indicate that floating mass should be tuned to be resonance with the incident wave frequency to optimize the harvested energy and total efficiency. The total efficiency can be found larger 45% thanks to resonance behavior. Moreover, due to non-linear behavior of the reactive force, a range of various optimum values for the equivalent mass and draft are found to be dependent on the incident wave frequency.

In realistic condition, stretch ratio of DEAP material is limited by the mechanical breakdown value (about 1.22). Therefore, the buoy mass must be controlled to desire the given value. The ideal buoy masses found by simulation for case 1 and case 2 are about 335 kg and 168 kg, respectively. Simulation results in case 2 show that the harvested energy is about 3 J after 100 s and the ideal total efficiency can reach higher 25%.

Future works involve in control strategies to optimize the harvested energy. A variable supplementary masses will be studied to apply in the PTO system, also the reactive force will be considered to optimize the hydrodynamic performance. Then, the proposed WEC is investigated under irregular wave. An appropriate wave spectrum will be selected to carry out the simulation. A simple test rig can be fabricated and tested in the water tank in the Research Institute of Small & Medium Shipbuilding (RIMS). In addition, some DE materials with larger strain capacity and higher energy density will be studied for increasing the output power.

ACKNOWLEDGEMENT

This work was partly supported by the New & Renewable Energy of the Korea Institute of Energy Technology Evaluation and Planning (KETEP) grant funded by the Korea government Ministry of Trade, Industry and Energy (G031518511) and by the project titled ‘R&D center for underwater construction robotics’, funded by the Ministry of Oceans and Fisheries (MOF) and Korea Institute of Marine Science & Technology Promotion (KIMST), Korea (PJT200539).

REFERENCES

1. Zuo, L. and Tang, X., “Large-Scale Vibration Energy Harvesting,” Journal of Intelligent Material Systems and Structures, Vol. 24, No. 11, pp. 1405-1430, 2013.
2. Antonio, F. D. O., “Wave energy Utilization: A Review of the Technologies,” Renewable and Sustainable Energy Reviews, Vol. 14, No. 3, pp. 899-918, 2010.
3. López, I., Andreu, J., Ceballos, S., de Alegría, I.M., and Kortabarria, I., “Review of Wave Energy Technologies and the Necessary Power-Equipment,” Renewable and Sustainable Energy Reviews, Vol. 27, No. pp. 413-434, 2013.
4. Faizal, M., Ahmed, M. R., and Lee, Y.-H., “A Design Outline for Floating Point Absorber Wave Energy Converters,” Advances in Mechanical Engineering, Vol. 6, Paper No. 846097, 2014.
5. Leclerc, J., Dumee, P., Kimoulakis, N., and Kladas, A., “Advanced Modeling and Control of a Wave Energy Conversion System,” Proc. of 20th International Conference on Electrical Machines (ICEM), pp. 2041-2045, 2012.
6. Nam, B. W., Hong, S. Y., Park, J., Shin, S. H., Hong, S. W., and Kim, K. B., “Performance Evaluation of the Floating Pendulum Wave Energy Converter in Regular and Irregular Waves,” International Society of Offshore and Polar Engineers, Vol. 24, No. 1, pp. 45-51, 2014.
7. Kamizuru, Y., Verdegem, L., Erhart, P., Langenstein, C., Andren, L., Lenßen, M., and Murrenhoff, H., “Efficient Power Take-Offs for Ocean Energy Conversion,” Proc. of the 4th International Conference on Ocean Energy, 2012.
8. Liao, Y. and Sodano, H. A., “Structural Effects and Energy Conversion Efficiency of Power Harvesting,” Journal of Intelligent Material Systems and Structures, Vol. 20, No. 5, pp. 505-514, 2009.
9. Abdi, H., Mohajer, N., and Nahavandi, S., “Human Passive Motions and a User-Friendly Energy Harvesting System,” Journal of Intelligent Material Systems and Structures, Vol. 25, No. 8, pp. 923-936, 2014.
10. van den Ende, D. A., Groen, W. A., and van der Zwaag, S., “Robust Piezoelectric Composites for Energy Harvesting in High-Strain Environments,” Journal of Intelligent Material Systems and Structures, Vol. 24, No. 18, pp. 2262-2269, 2013.
11. Usha, S. and Sreekumar, M., “Elastic Behaviour of Deap Film in the Development of Actuators,” Procedia Engineering, Vol. 41, pp. 1154-1161, 2012.
12. Wissler, M. and Mazza, E., “Electromechanical Coupling in Dielectric Elastomer Actuators,” Sensors and Actuators A: Physical, Vol. 138, No. 2, pp. 384-393, 2007.
13. Pelrine, R., Kornbluh, R. D., Eckerle, J., Jeuck, P., Oh, S., Pei, Q., and Stanford, S., “Dielectric Elastomers: Generator Mode Fundamentals and Applications,” Proc. of SPIE's 8th Annual International Symposium on Smart Structures and Materials, Vol. 4329, pp. 148-156, 2001.
14. Czech, B., van Kessel, R., Bauer, P., Ferreira, J. A., and Wattez, A., “Energy Harvesting using Dielectric Elastomers,” Proc. of 14th International Power Electronics and Motion Control Conference (EPE/PEMC), pp. S4-S18, 2010.

15. Ahnert, K., Abel, M., Kollosche, M., Jørgensen, P. J., and Kofod, G., "Soft Capacitors for Wave Energy Harvesting," Journal of Materials Chemistry, Vol. 21, No. 38, pp. 14492-14497, 2011.

16. Meddad, M., Eddiai, A., Guyomar, D., Belkhiat, S., Hajjaji, A., et al., "Evaluation by Fast Fourier Transforms Analysis of Energy Harvesting in Electrostrictive Polymers Driven by An Electric Field And A Mechanical Excitation," Journal of Intelligent Material Systems and Structures, Vol. 24, No. 4, pp. 411-420, 2012.

17. Graf, C., Hitzbleck, J., Feller, T., Clauberg, K., Wagner, J., et al., "Dielectric Elastomer–based Energy Harvesting: Material, Generator Design, and Optimization," Journal of Intelligent Material Systems and Structures, Vol. 25, No. 8, pp. 951-966, 2014.

18. Wang, H., Zhu, Y., Wang, L., and Zhao, J., "Experimental Investigation on Energy Conversion for Dielectric Electroactive Polymer Generator," Journal of Intelligent Material Systems and Structures, Vol. 23, No. 8, pp. 885-895, 2012.

19. Chiba, S., Waki, M., Wada, T., Hirakawa, Y., Masuda, K., and Ikoma, T., "Consistent Ocean Wave Energy Harvesting using Electroactive Polymer (Dielectric Elastomer) Artificial Muscle Generators," Applied Energy, Vol. 104, pp. 497-502, 2013.

20. Graf, C., Aust, M., Maas, J., and Schapeler, D., "Simulation Model for Electro Active Polymer Generators," Proc. of 10th IEEE International Conference on Solid Dielectrics (ICSD), pp. 1-4, 2010.

21. Jean-Mistral, C., Basrour, S., and Chaillout, J., "Modelling of Dielectric Polymers for Energy Scavenging Applications," Smart Materials and Structures, Vol. 19, No. 10, Paper No. 105006, 2010.

22. Antoniadis, I., Venetsanos, D., and Papaspyridis, F., "DIESYS - Dynamically Non-Linear Dielectric Elastomer Energy Generating Synergetic Structures: Perspectives and Challenges," Smart Materials and Structures, Vol. 22, No. 10, Paper No. 104007, 2013.

23. Krakovský, I., Romijn, T., and de Boer, A. P., "A Few Remarks on the Electrostriction of Elastomers," Journal of Applied Physics, Vol. 85, No. 1, pp. 628-629, 1999.

24. Martins, P., Natal Jorge, R. M., and Ferreira, A. J. M., "A Comparative Study of Several Material Models for Prediction of Hyperelastic Properties: Application to SiliconeRubber and Soft Tissues," Strain, Vol. 42, No. 3, pp. 135-147, 2006.

25. Wissler, M. and Mazza, E., "Modeling and Simulation of Dielectric Elastomer Actuators," Smart Materials and Structures, Vol. 14, No. 6, pp. 1396-1402, 2005.

26. Binh, P. C., Nam, D. N. C., and Ahn, K. K., "Modeling and Experimental Investigation on Dielectric Electro-Active Polymer Generator," Int. J. Precis. Eng. Manuf., Vol. 16, No. 5, pp. 945-955, 2015.

27. Binh, P. C., Nam, D. N. C., and Ahn, K. K., "Modeling and Experimental Analysis of an Antagonistic Energy Conversion using Dielectric Electro-Active Polymers," Mechatronics, Vol. 24, No. 8, pp. 1166-1177, 2014.

28. Alves, M., Traylor, H., and Sarmento, A., "Hydrodynamic Optimization of a Wave Energy Converter using a Heave Motion Buoy," Proc. of the 7th European Wave and Tidal Energy Conference, pp. 11-14, 2007.

29. Binh, P. C., Truong, D. Q., and Ahn, K. K., "A Study on Wave Energy Conversion using Direct Linear Generator," Proc. of 12th International Conference on Control, Automation and Systems (ICCAS), pp. 64-69, 2012.

30. Falnes, J., "Ocean Waves and Oscillating Systems," Cambridge University Press, 2004.